

Bio-Inspired Locomotion for Unmanned Underwater Vehicles

J.D. Geder,¹ R. Ramamurti,¹ M. Pruessner,² B. Ratna,² J. Palmisano,³ and W. Sandberg⁴

¹Laboratories for Computational Physics and Fluid Dynamics

²Center for Bio/Molecular Science and Engineering

³NOVA Research, Inc.

⁴SAIC, Inc.

Introduction: As greater levels of remote operation and autonomy are becoming possible, we are increasingly turning to robots for solutions in environments where it is infeasible or unsafe to send human or animal operators to perform a specific function. In fact, the Naval Science and Technology Strategic Plan has singled out autonomy and unmanned systems as an important research focus area to enable future Navy operations.

In the undersea realm, unmanned vehicles are currently being deployed for military operations in mine and antisubmarine warfare, scientific operations for mapping and analyzing various underwater environments, and commercial operations in the oil and gas industry, among others. However, of all the missions in which traditional propeller-driven unmanned underwater vehicles (UUVs) have been successfully deployed, none have been in cluttered, nearshore environments where precise positioning and small-radius maneuvers are required in the presence of waves and alternating currents. To tackle the problems that propeller-driven vehicles have in this critical environment, researchers at NRL¹ and elsewhere have studied the fin force production mechanisms used by various fish species to understand how these organisms achieve their high levels of controllability.

Fin Development: At NRL we have drawn inspiration from a particular coral reef fish, the bird wrasse, to develop an actively controlled curvature robotic fin. The fin consists of five ribs, each actuated to create a spanwise (from fin root to tip) curvature (Fig. 1(a)). The actuation of each of the five ribs in turn creates a chordwise (from fin leading to trailing edge) curvature (Fig. 1(b)). Active control of fin curvature is a unique feature necessary for enabling generation of desired force vectors for propulsion and control.

In addition to fin curvature, other fin parameters contribute to force generation. Through a combination of computational and empirical analyses, we have modeled the effects of these parameters on fin force generation.² Initial studies on a single isolated fin served to characterize thrust and lift production as functions of fin curvature, flapping frequency and amplitude, fin

stroke angle bias, and freestream flow velocity. Subsequent studies on multiple fins have added to the initial models by quantifying the effects of spacing between fins and stroke angle phase differences on thrust and lift generation. Further, all of the studied stroke parameters are coupled, and our models have been derived to sufficiently capture how simultaneous variations in multiple parameters affect force production.

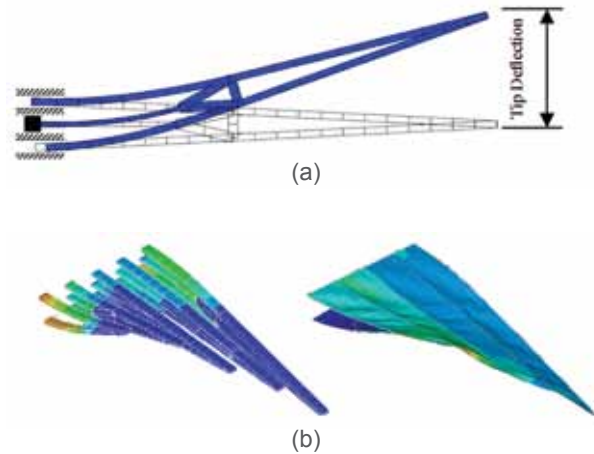


FIGURE 1

(a) One of the five fin ribs showing the actuation of the structure at the rib base creating a deflection at the rib tip. This creates spanwise curvature in each rib. (b) The entire fin showing each of the five ribs deflected with different directions and magnitudes. This creates chordwise curvature across the fin.

Vehicle Development: Following the development and modeling of the bio-inspired robotic pectoral fins, we designed and built a UUV to demonstrate the capability of these fins as effectors of vehicle propulsion and control (Fig. 2). This NRL Bio-UUV includes a basic suite of sensors for testing and validation including an inertial measurement unit, compass, depth gauge, and sonar range finder. It also has onboard power and an onboard processor for determining actuator outputs from the sensor measurements, as well as a radio for wireless data transmission in real time. The four-fin design enables vehicle pitch and roll stability control, tight radius yaw maneuvers, and an opportunity to improve thrust generation from manipulation of multiple fin flow interactions.

Performance: Simulations of vehicle performance have been carried out using the high-fidelity fin models described, along with a 6-degree-of-freedom vehicle model, and sensor and actuator models. Validation of these models through comparison of simulation results with experimental vehicle results demonstrates that we have developed a tool with which to conduct future fin and fin-driven vehicle designs (Fig. 3). With a forward



(a)



(b)

FIGURE 2

(a) Functional prototype of, and (b) surface pressure distribution on, the NRL Bio-UUV with four actively controlled curvature pectoral fins.

speed of about one-half meter per second (greater than one body length per second), a zero turn radius,² and ability to move vertically through a column of water,³ the NRL Bio-UUV is capable of the precise trajectory control needed in cluttered environments.

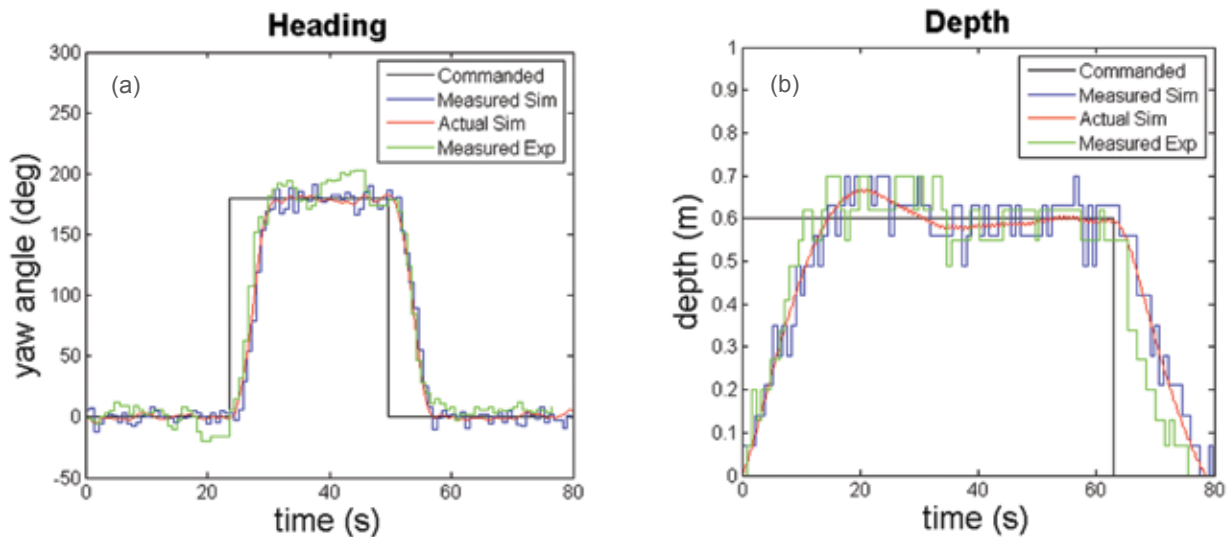


FIGURE 3

Comparison of simulated and experimental vehicle performance in (a) heading and (b) depth responses. Agreement of these results validates the models derived for the fin and vehicle.

Summary: Active-curvature control of a flapping fin has enabled the generation of desired three-dimensional force vectors, thereby removing the need for multiple thrusters. The results of our vehicle studies have proven the NRL fin and the subsequent NRL Bio-UUV as capable technologies in our drive to develop an unmanned vehicle for performing critical nearshore operations in confined environments. Further, the tools used to develop the fin and vehicle models can be applied to guide future designs aimed at achieving specific performance metrics. In short, NRL's research in bio-inspired underwater locomotion is laying the foundation for successful UUV operations in highly dynamic nearshore environments.

[Sponsored by the NRL Base Program (CNR funded)]

References

- ¹ R. Ramamurti and W.C. Sandberg, "Computations of Insect and Fish Locomotion with Applications to Unconventional Unmanned Vehicles," *AIAA J.* **46**(9), 2178–2190 (2008).
- ² J.D. Geder, R. Ramamurti, J. Palmisano, M. Pruessner, B. Ratna, and W.C. Sandberg, "Four-Fin Bio-Inspired UUV: Modeling and Control Solutions," ASME International Mechanical Engineering Congress and Exposition, Denver, CO, Nov. 11–17, 2011.
- ³ J.D. Geder, R. Ramamurti, J. Palmisano, B. Ratna, and W.C. Sandberg, "Dynamic Performance of a Bio-Inspired UUV: Effects of Fin Gaits and Orientation," 17th International Unmanned Untethered Submersible Technology Conference, Portsmouth, NH, Aug. 21–24, 2011.

Extending Optical Visibility Prediction Range with the Help of Acoustics

W. Hou,¹ E. Jarosz,¹ S. Woods,² W. Goode,¹ and A. Weidemann¹

¹Oceanography Division

²ASEE Postdoctoral Research Associate

Improving Diver Visibility: Enhanced diver visibility, particularly in coastal ocean waters, benefits not only warfighters executing mine warfare (MIW) and antisubmarine warfare (ASW) missions, but also many civilian applications, including search and rescue operations, underwater inspection, and tourism. Turbidity of the water column (or water clarity) is the single largest predictor of diver visibility. However, other factors, such as underwater turbulence, can affect diver visibility and lead to erroneous predictions and potentially significant consequences. Turbulence structures are exceptionally challenging to characterize over long ranges, but this characterization is key in predicting the resolution and range of electro-optical (EO) systems for mine identification and other underwater missions. The performance of long range EO systems can be adversely impacted by the difficulty of quantifying turbulence structures at large scales over short periods of time. This gap in supplying the turbulence information can be addressed by exploiting acoustic backscattering signals. We developed a novel approach based on this idea and used data from the recent Skaneateles Optical Turbulence Exercise (SOTEX, July 2010) to validate the results.

How Can Acoustic Signals Help Optics? In conducting research related to ASW needs, the Navy has developed strong capabilities in acoustical characterization of underwater environments. It would be very helpful if such information could be leveraged into optical models, in effect using the longer reach from the acoustical systems to enhance the higher resolutions of the optics. We hypothesize that the same turbulent microstructures in the ocean that impact sound propagation and scattering also impact optical scattering due to index of refraction variations (optical turbulence), despite the differences in pressure waves versus electromagnetic waves. The acoustical scattering cross section (σ) from turbulence microstructures for a given sound frequency has been shown to be proportional to the first-order derivatives of the one-dimensional spectrum of sound speed fluctuations.^{1,2} This can be further expressed as a function of vertical wavenumber, turbulent kinetic energy dissipation rate (ϵ , TKED), and the temperature variance dissipation rate (χ , TD), in a combined spectrum including buoyancy-dominated, inertial, and Batchelor subranges.² Our recently

developed EO imaging model showed that the optical turbulence intensity (S_n) is also a function of TKED and TD.³ We examined the relationships between σ and S_n using data collected during the SOTEX field campaign, in one of the Finger Lakes of upstate New York, where strong stratification due to the thermocline was present in clear waters.

Sample measurements of TKED and TD from July 30 can be seen in Fig. 4. The corresponding derived optical turbulence intensity coefficient (S_n) and acoustical scattering cross section (σ) are shown in Fig. 5. Since our focus here is to explore the shape of the profiles and examine their correlation, relative units are used in the figures. We notice the general trend of stronger optical turbulence at or near the thermocline around 10 to 15 m deep. The strong turbulence layer can be observed in both the TKED and TD rate profiles throughout

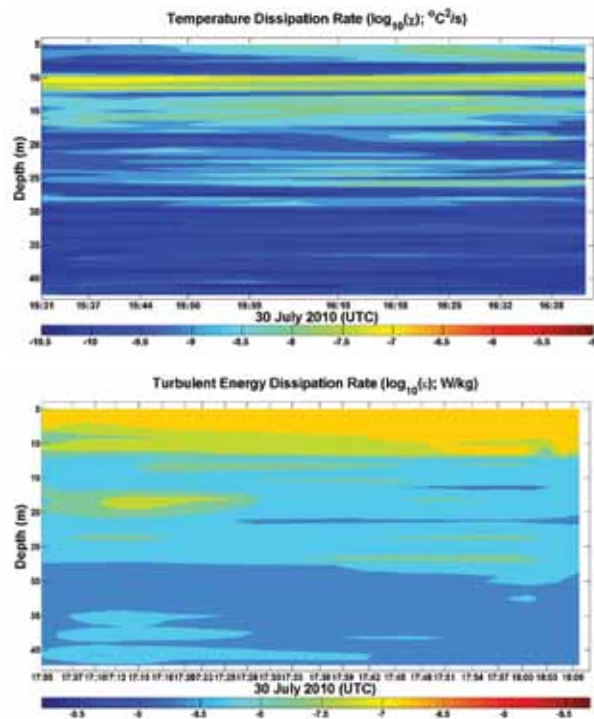


FIGURE 4

Interpolated vertical microstructure profiler (VMP) measurements of TKED rate, ϵ (m^2/s^3) (bottom) and TD rate, χ ($^\circ\text{C}^2/\text{s}$) (top), showing the spatial and temporal variability of the turbulence field for July 30, 2010, during SOTEX.

the exercise. It is encouraging, while not surprising, to see that indeed both the optical turbulence intensity coefficient and the acoustic scattering cross section follow the same trend, shown in the lower part of Fig. 5. This trend is predominantly determined by the temperature dissipation rate structure. The closely related trend observed in Fig. 5 is more obvious when S_n is plotted against σ in Fig. 6, and correlation coefficients are calculated. These graphs support our hypothesis

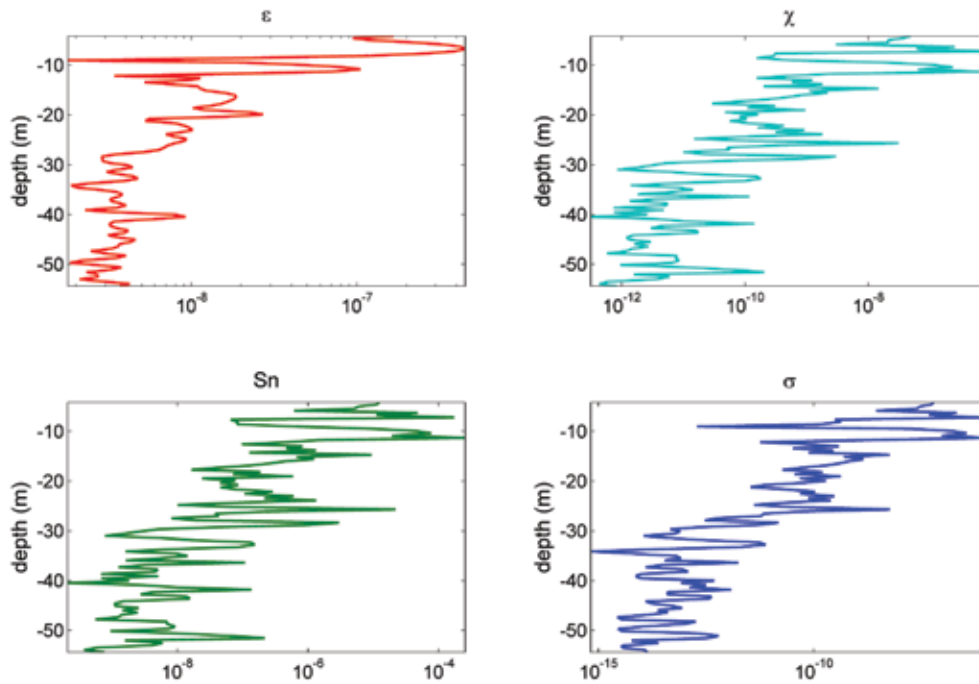


FIGURE 5 VMP turbulence measurements of TKED (ϵ) and TD rates (χ), optical turbulence intensity (S_n) and acoustical scattering cross section (σ) on July 30, 2010. The unit for ϵ is m^2/s^3 , while χ is $^\circ C^2/s$. S_n and σ are not calibrated.

that a positive correlation exists between the optical turbulence intensity and acoustic scattering cross sections, as demonstrated by the correlation coefficients of 0.93 (multiple days during the exercise ranged from 0.86 to 0.99 using a log-log scale). The result shown here implies a strong relationship between the optical and acoustical signals impacted by turbulent conditions. It is worth mentioning that due to differences in deployment requirements to quantify dissipation rates of TKED and TD, profiles have been interpolated to the nearest points in space and time, in order to

have co-incident measurements at desired depth to calculate impacts on both the optics and acoustics. This procedure likely introduces undesired variances in the presented figures. Efforts are under way to investigate and minimize these noise terms.

Summary: A novel approach that uses acoustic scattering returns to estimate long-range optical signal degradation caused by turbulence is described. Data obtained during the SOTEX field campaign validated the relationship between the acoustic and the optical returns. A strong correlation (>0.9) can be seen during multiprofile observations. When combined with the current active EO imaging system performance model for the Navy's mine hunting systems, this result enables us to significantly enhance prediction accuracy, as it addresses contributions from turbulence over long ranges, in the presence of particle contributions, for the first time.

[Sponsored by the NRL Base Program (CNR funded)]

References

- ¹ T. Ross and R. Lueck, "Sound Scattering from Oceanic Turbulence," *Geophys. Res. Lett.* **30**, 1343 (2003).
- ² L. Goodman, "Acoustic Scattering from Ocean Microstructure," *J. Geophys. Res.* **95**, 11557-11573 (1990).
- ³ W. Hou, "A Simple Underwater Imaging Model," *Opt. Lett.* **34**, 2688-2690 (2009).

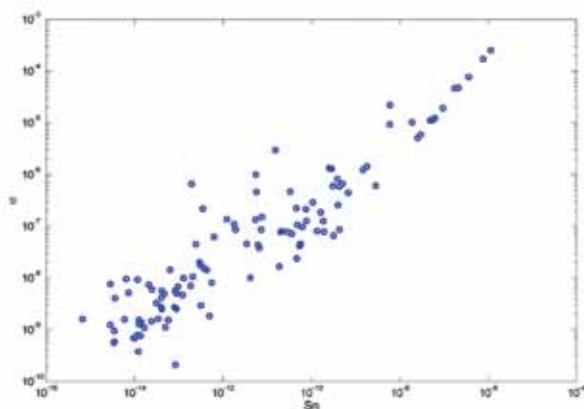


FIGURE 6 Optical turbulence intensity (S_n) vs acoustical scattering cross section (σ) for July 30, 2010. Correlation coefficient is 0.93 on the log-scale plot shown.

Tomographic Particle Image Velocimetry of Bottom Boundary Layer Processes

J. Calantoni¹ and I.M. Sou²

¹ Marine Geosciences Division

² National Research Council Postdoctoral Fellow

Introduction: Boundary layer processes are dominated by the interaction between fluid turbulence and immersed particles. Fluid turbulence causes airplane travel to be uncomfortable, generates dust storms, and drives sediment transport responsible for beach erosion. Developing a set of governing equations for flow and behavior of granular and granular-fluid mixtures has been a long-standing scientific challenge. Here we bring a relatively new technology to bear on an old problem by using state-of-the-art optical techniques for measuring fluid flow and the velocities of grains immersed in the fluid (e.g., sand in water). Our focus is on understanding how fluid turbulence entrains and deposits sediments on seafloor, estuarine, and river beds. Timely and accurate characterization of the bottom boundary layer in these operational environments is critical to improving the utilization of Navy sensors and forecasting models.

Experimental Facility: Measurements are performed in the laboratory on boundary layer flows generated within a small oscillatory flow tunnel (S-OFT). The S-OFT is equipped with a piston drive system to simulate the action of fluid flow at the seafloor under waves in shallow water. As a wave passes, the sea surface moves up and down, which drives fluid motion back and forth over the seafloor. Here, our tunnel test section contains a sediment well that is filled with beach sand. The motion of the water over the sediments generates fluid turbulence, sediment transport, and sometimes forms sand ripples as shown in Fig. 7. Additionally, the S-OFT contains a pump to drive steady flow that may be combined with the oscillatory flow. A pair of sediment wells on each side of the test section is used to collect transported sediments.

Tomographic particle image velocimetry (Tomographic PIV) is a remote sensing technique used in the laboratory to measure the time-resolved three-dimensional three-component (3D-3C) velocity vector field.¹ Our system uses four high-speed video cameras and a high-repetition laser. Laser light illuminates the flow from above while the cameras image through the sidewall of the S-OFT. The flow is seeded with fine particulate material that essentially follows the motion of the fluid while scattering laser light. Image pairs are acquired at a very precise and narrow time interval.

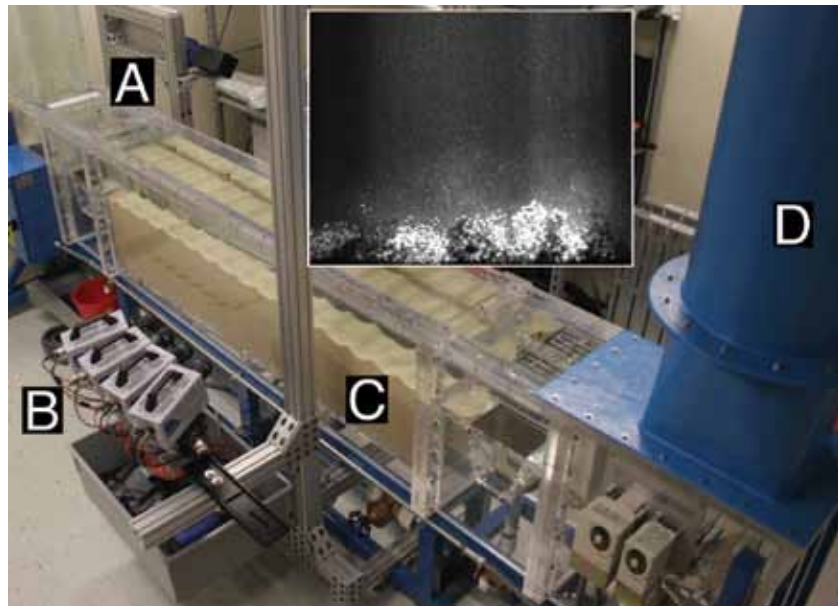


FIGURE 7

Shown is a photograph of the small oscillatory flow tunnel (S-OFT). (A) The laser head is mounted near the open head box shown in the upper left corner. (B) The bank of video cameras used to image the flow is located to the left of the test section. (C) Water flows back and forth across the test section driving boundary layer flow where sand ripples have formed. (D) The oscillatory flow is driven by vertical piston motion contained in the blue headbox that is partially visible on the right side of the image. The inset shows an example of a raw image acquired by one of the video cameras. In the inset, the brighter and larger bed material is readily distinguishable from the fine particulate material above that is used to seed the flow.

Computationally intensive image processing allows for a construction of the 3D-3C velocity vector field within a relocatable measurement volume (up to 1000 cm³). The system has temporal resolutions from 50 to 100 Hz with millimeter spatial resolution.

Vortex Measurements: The 3D-3C velocity data allow us to visualize the time-dependent and three-dimensional characteristics of turbulent coherent structures such as vortex stretching and bending. Preliminary measurements show a snapshot of a vortex being shed from an idealized sand ripple (Fig. 8). The vortex shown in the upper right panel is depicted by the swirling strength of the flow. The contours of swirling strength illuminate the complex structure of the turbulence at a specific instant in time. Here, the swirling strength is a scalar quantity that allows one to locate the cores of rotating structures in turbulent flows. In the upper left panel, the velocity vectors also highlight the rotation of the flow. The lower panel is an estimate of the instantaneous bed shear stress. Bed shear stress is a quantity commonly used to estimate sediment

transport, but has been notoriously difficult to measure directly.²

Research Applications: The data obtained in our experimental facility will be used to validate simulations that predict the fine-scale structure of fluid turbulence responsible for sediment entrainment and deposition. We pursue these studies because we believe that ultimately all large-scale phenomena are governed by physics at the microscale. For example, all changes in bathymetry in the littoral, estuaries, and rivers begin with small amounts of sediment being entrained and deposited from local areas of the bottom. We are currently resolving the 3D-3C Eulerian flow field very near the Kolmogorov length scale, which represents the fundamental length scale for fluid turbulence. Ongoing experiments are focused on phase separation where we attempt to discriminate with a single set of images between seeded particles that allow us to image the flow and the actual sediment particles on the bed (see inset to Fig. 7).

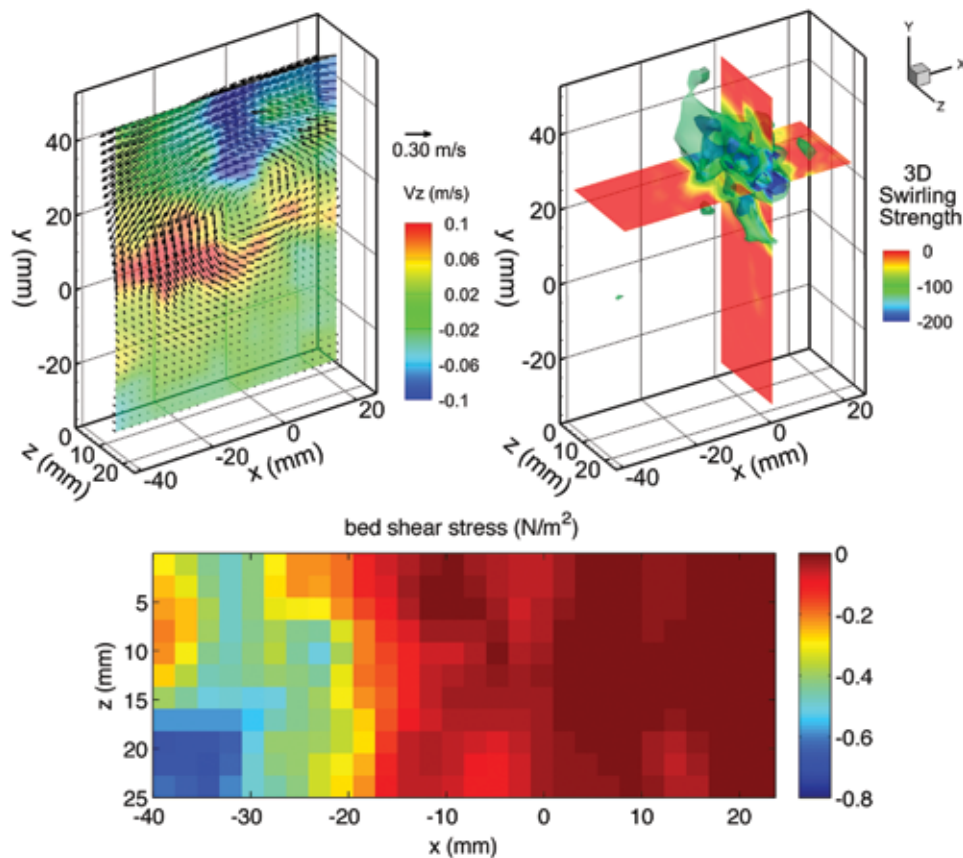


FIGURE 8

Shown is a snapshot of a vortex being shed from an idealized sand ripple. The swirling strength is contoured in the upper right panel. The planes roughly intersect the dominant vortex core. A slice of the three-dimensional velocity is shown in the upper left panel where the color contours indicate velocity in and out of the plane, while the vectors highlight the rotation of the flow. The lower panel is an estimate of the instantaneous bed shear stress.

Summary: The experimental facilities and preliminary measurements described here demonstrate a unique capability that will allow us to make detailed measurements of the fundamental processes driving the fluid-sediment bottom boundary in the littoral, estuaries, and rivers. Measurements will be used to validate fluid-sediment phase closure relations in highly resolved three-dimensional models for the direct numerical simulation of small-scale sand ripples. Long-term research is focused on development of robust models to forecast temporal and spatial changes in the littoral, estuarine, and river bottom boundary layers.

Acknowledgments: Equipment was purchased through the Capital Procurement Program of the Naval Research Laboratory. We thank Mr. Sigurd Anderson from Engineering Laboratory Design, Inc. for his excellent service in the design and fabrication of the small oscillatory flow tunnel. We thank Dr. Callum Gray from LaVision, Inc. for his tireless efforts to install and calibrate the Tomo-PIV system.

[Sponsored by ONR]

References

- ¹ G.E. Elsinga, F. Scarano, B. Wieneke, and B.W. van Oudheusden, "Tomographic Particle Image Velocimetry," *Experiments in Fluids* **41**, 933–947 (2006).
- ² J.K. Seelam, P.A. Guard, and T.E. Baldock, "Measurement and Modeling of Bed Shear Stress Under Solitary Waves," *Coastal Engineering* **58**(9), 937–947 (2011).

Rapid Autonomous Fuel Transfer for USVs

G.P. Scott and C.G. Henshaw
Spacecraft Engineering Department

Introduction: The Naval Research Laboratory has developed a prototype robotic system to autonomously refuel unmanned surface vehicles (USVs) while on the open sea. Even at an active sea state of 3.25 (wave heights over 1 m), the robotic system can successfully transfer fuel from the host vehicle.

Background: Refueling Navy vessels in the open sea is a challenging prospect. Large, conventional vehicles require huge cranes to hoist the required fuel lines and associated cabling between the two vessels. Sailors are required to manually attach and detach the required cabling and react appropriately to anomalies.

For USVs, the difficulty is even greater, as these vehicles are more significantly affected by the sea state. If the ships veer too far apart or communication breaks

down during the process, lines can snap and Sailors involved in the process can be injured or killed.

The Naval Research Laboratory's Space Robotics Laboratory and Clemson University have developed an autonomous robotic methodology for refueling USVs. This article addresses the development, control, and testing of a robotic refueling system.

Robotic Refueling System: The team proposed a robotic system that can be controlled manually by Sailors aboard the refueling vehicle or autonomously through visual tracking of the fuel receptacle. This robotic system is made up of two primary segments: one rigid and the other flexible.

The first is a rigid industrial manipulator that can provide rapid and accurate movement to respond quickly to the movement of the fuel tank on the USV. The Mitsubishi PA10-7CE industrial robotic arm was selected for this task due to its extensive use by NRL.

The second is a compliant pneumatic manipulator that provides a flexible connection between the rigid arm and the fuel receptacle to minimize the possibility of damage to either arm or the vessel. The Clemson-designed Octarm was selected due to its successful operation in a previous initiative sponsored by the Defense Advanced Research Projects Agency (DARPA).

Together, the PA10 and the Octarm make up the robotic refueling system. Shown in Fig. 9, this system has a maximum reach of nearly 2 m. In total, the system has 7 rigid degrees of freedom and 9 pneumatic degrees of freedom.

In between the PA10 and the Octarm is a down-pointing digital video camera that targets a tracking fiducial on the USV. The robotic arm uses this camera and a visual servoing algorithm to autonomously move the system to a configuration that pinpoints the end effector above the fuel receptacle so that it can dock to transfer fuel.

Fuel Transfer: The fuel transfer system is designed and prototyped to transfer fuel to a target fuel tank on the USV without the need for direct human intervention.

The system provides a self-aligning magnetic connection between the host and target systems. Within this magnetic connection is a transferrable "puck" that is attracted more strongly toward the target system than the host system. This magnetic differential allows the puck to connect to the target system and, in the case of waves pushing the systems apart, only separate from the weaker magnetic connection on the host system.

A flexible hose is connected through the puck to transfer fuel between the host system and the target system. In the event that the magnetic connection to the robotic system is lost, the flexible hose has signifi-



FIGURE 9
The combined robotic refueling system, including the PA10 and Octarm.

cant slack in the line to allow for it to be unaffected by shifting distances between the target and host systems. Figure 10 shows the fuel puck attaching to the fuel receptacle prior to fluid transfer.

Test Results: To test the robotic refueling system, it was mounted to a support truss and extended over a wave tank at the U.S. Army Aberdeen Test Center. A U.S. Navy Sea Fox unmanned surface vehicle was used as the target vehicle, on which a custom refueling platform was built to allow the robotic system to target the fuel tank and transfer fluid. This full configuration is shown in Fig. 11.

Tests were conducted at varying wave intervals from sea state 0 (calm seas) up to sea state 3.25 (with wave height over 1 m). In each wave state, multiple robotic docking approaches were performed, both autonomously and with manual operators controlling the movement and docking procedures of the robotic refueling system.

Preliminary tests were conducted with prototype hardware where 102 docking runs were performed. Of these, 74 were successful, providing a 73% success rate with the preliminary hardware. During the final test demonstration, 59 tests were conducted at varying wave states between sea states 2.0 and 3.25. Of these, 36

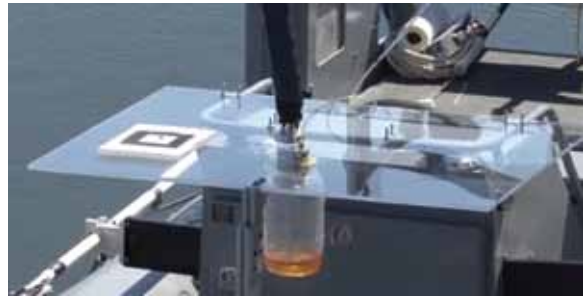


FIGURE 10
The fuel puck (in center of photo) magnetically attaching to the fuel receptacle in preparation for fluid transfer.



FIGURE 11
The full system tested at the U.S. Army Aberdeen Test Center wave tank.

manual tests were successful (95%) and 17 autonomous tests were successful (80%).

These results far exceeded DARPA's program requirements of demonstrating autonomous and manual docking under sea state 2.0 conditions by successfully docking and transferring fluid under sea state 3.25 conditions.

Acknowledgments: NRL acknowledges the full team that supported this project, consisting of the Space and Naval Warfare Systems Command (SPAWAR), Science Applications International Corporation (SAIC), the Naval Research Laboratory (NRL), and Clemson University, each focusing on a different area of the challenge. This project was funded under the DARPA Rapid Autonomous Fuel Transfer Seedling Program.

[Sponsored by DARPA]

